Numerical Investigation on Load Redistribution Capacity of Flat Slab Substructures to Resist Progressive Collapse

Yun-Hao Weng[1], Kai Qian[1*], Feng Fu[2], and Qin Fang[3]

[1] College of Civil Engineering and Architecture, Guangxi University, 100 Daxue Road, China, 530004.

[2] School of Mathematics, Computer Science and Engineering, City, University of London, London, EC1V 0HB UK

[3] Army Engineering University, Nanjing 210007, Jiangsu, Peoples R China

Abstract: To study the load redistribution capacity of reinforced concrete (RC) flat slab structures subjected to a middle column loss scenario, high fidelity finite element (FE) models were built using commercial software LS-DYNA. The numerical models were validated by experimental results. It is found that the continuous surface cap model (CSCM) with an erosion criterion considering both the maximum principal and shear strain could effectively predict the punching shear failure at slab-column connections. The validated FE models were employed to investigate the effect of boundary conditions, amount of integrity reinforcement, and slab thickness on the load redistribution capacity of flat slab structures. Furthermore, multi-story RC flat slab substructures were built to capture the load redistribution behavior of different floors. Parametric studies indicate that ignoring the constraints from surrounding slabs may underestimate the load redistribution capacity of the flat slab substructures. Therefore, it is suggested that in future numerical or experimental studies, rigid horizontal constraints should be applied at the slab edge of the substructure to well represent the constraints from surrounding slabs. In addition, it is also found that the amount of integrity reinforcement would significantly affect the post-punching performance of flat slab structures. It is suggested that the minimum integrity reinforcement ratio should be 0.63 %.

Keywords: Progressive collapse; Flat slab substructures; Quasi-static; Punching shear; Load resisting mechanism

* Corresponding author. Tel.: 65+67905292, E-mail address: qiankai@gxu.edu.cn

1. Introduction

An initial local failure of supporting components due to accidents may lead to a disproportionate collapse of the structure, which is defined as disproportionate collapse or progressive collapse. The consequence of casualties caused by progressive collapse event is very tragic. Progressive collapse attracted public attention first after the collapse of Ronan Point apartment in 1968 and raised concerns by design regulators after the catastrophic consequences of the Murrah Federal Building in Oklahoma City in 1995 and World Trade Centre in New York City in 2001. Several design guidelines (DoD 2009 [1]; GSA 2003 [2]; ASCE/SEI-10 2010 [3]; COST Action TU0601 2008 [4]) were proposed accordingly. Moreover, these progressive collapse incidents also attracted a large number of researchers to investigate the load redistribution behavior and load resisting mechanisms of the structures subjected to different column removal scenarios. In the past decade, several studies have been conducted to study progressive collapse based on the alternative load path method stipulated in DoD [1] and GSA [2].

Su et al. [5] tested twelve reduced-scale RC beam-column sub-assemblages to investigate the effects of beam reinforcement ratio, span-to-depth ratio, and loading rate on the compressive arch action of RC frames. Two one-half scaled sub-assemblages with seismic and non-seismic detailing were tested by Yu and Tan [6] to evaluate the effects of seismic design on behavior of RC frames in resisting progressive collapse. Feng et al. [7] evaluated the behavior of precast concrete structures to resist progressive collapse by using a three-dimensional FE model. Fascetti et al. [8] proposed a procedure to evaluate the robustness of RC frame against progressive collapse based on a macro-model simulation. Livingston et al. [9] carried out a series of pushdown analysis to quantify the effects of structural characteristics (e.g. axial stiffness at the beam boundaries, amount of integrity reinforcement at bar cut-off locations, etc) on progressive collapse resistance of frames. High fidelity solid-element-based numerical models were used by Yu et al. [10] to investigate the robustness of RC beam-slab substructures under perimeter column removal scenarios. Shan et al. [11] tested two one-third scale, four-bay by two-story RC frame to investigate the effects of infilled wall on the load resisting mechanisms of RC frames. Based on their tests, it was concluded that infilled walls could enhance the load resisting capacity of RC frames significantly due to more alternative load paths provided. However, the infilled walls might decrease the ductility of the frames. Sadek et al. [12] tested four (two RC and two steel) full-scale beam-column sub-assemblages subjected to the loss of an interior column to provide insight into the mobilization of catenary action. Qian and Li [13] tested two series of six specimens (with and/or without RC slab) to quantify the contribution of RC slabs in resisting progressive collapse under a corner column loss scenario. It was found that RC slabs could improve the ultimate load resisting capacity by 63 %. Pham et al. [14] investigated the effect of different loading patterns and boundary conditions on tensile membrane action (TMA) of beam-slab systems. Lu et al. [15] and Ren et al. [16] conducted a number of one-third scaled specimens to investigate the effects of RC slabs on the behavior of RC frames to resist progressive collapse caused by either an edge or an interior column loss scenario. Feng et al. [17] used the probability density evolution method to evaluate the robustness of RC beam-column sub-assemblage under a column missing scenario.

Flat slab floor system has been widely used in tall and multi-story buildings, due to its long span and small thickness features. However, there is relatively little attention paid on flat slab structures to resist progressive collapse. For flat slab structures, a column loss leads to load redistribution, result in the increase of bending moment and shear force at adjacent slab-column connections significantly. The likelihood of progressive collapse increases as no load redistribution in beams can be triggered in flat slab structures. This may cause collapse of the buildings such as of the incidents of Sampoong Department Store at Seoul, South Korea. Russell et al. [18] tested seven 1/3 scaled RC flat slab substructures subjected to the quasi-static or dynamic loading regimes. The experimental results showed that flat slabs could redistribute the loads effectively after a column lost. However, punching shear failure was a critical issue must be addressed seriously. Qian and Li [19, 20] and Ma et al. [21] conducted several series of tests to investigate the load resisting mechanisms and quasi-static behaviour of RC flat slab structures subjected to the loss of corner or interior column scenarios. Keyvani et al. [22] developed a new finite element modeling technique to simulate punching and post-punching behavior of flat plates. Moreover, the effects of compressive membrane action (CMA) on load resisting capacity of flat plate structures were also investigated by Keyvani et al. [22]. Liu et al. [23] proposed a macromodel for slab-column connections, which could be used to simulate the behaviour of flat slab or flat plate structures in resisting progressive collapse. Peng et al. [24] carried out a series of dynamic tests to study the dynamic response of flat plate substructure subjected to instantaneously removal of an exterior column. Qian et al. [25] conducted experimental and numerical studies to evaluate the dynamic response of flat slab structures subjected to different extents of initial local damage (one-column or two-column removal).

Due to the complexity of testing on multi-panel flat slab structures, the majority of existing experimental tests on progressive collapse resistance are single-storey substructures or sub-assemblages with simplified boundary condition (applying weights at the overhang to simulate the constraints from surrounding components [19-21, 24] or ignoring the constraints from surrounding components [18]), which is different from the real conditions in a building. It is necessary to conduct further studies to evaluate the effects of boundary condition on the behavior of flat slab substructures to mitigate progressive collapse. Moreover, due to excessive time and high cost for experimental studies, some of critical parameters could not be investigated by experimental studies. Therefore, developing an accurate numerical simulation method is imperative. In this paper, numerical simulation based on high fidelity FE models are developed using LS-DYNA. The FE models are validated by test results. Then, the validated FE models are used to quantify the effect of surrounding slabs and upper floors on the load redistribution capacity of flat slab substructure. In addition, for multi-storey flat slab buildings, the load redistribution ability of each floor was evaluated individually to reveal the difference of loading resisting mechanisms and load resisting contribution of each floor. Finally, the effects of integrity reinforcement and slab thickness on the load redistribution capacity of flat slab substructures are also investigated.

2. Experimental program and numerical validation

2.1. Brief of experimental program

To determine the possible load resisting mechanisms in flat slab structures to resist progressive collapse, a test program was conducted by Qian and Li [20]. An experimental program included three 1/4 scaled multi-panel flat slab substructures. The prototype of these specimens was designed according to provisions of ACI 318-11 [26]. The total dead load (DL) including the self-weight of the slab and the weights of infilled walls was assumed to be 8.0 kPa. The live load (LL) was assumed to be 3.0 kPa. Two specimens (ND and WD) from Qian and Li [20] are used to validate numerical models. These two flat slab substructures have identical dimensions and reinforcement details. One of the specimens has enhanced punching shear capacity due to the drop panels at slab-column connections. Table 1 gives the specimen properties while Fig. 1 shows the dimensions and reinforcement details of Specimen WD. As it can be seen from the figure, Specimen WD consists of a slab with dimension of 3750 mm×3750 mm×55 mm, nine columns including one interior column and eight surrounding columns, and nine drop panels with size of 450 mm×450 mm×35 mm. The cross-section of columns was 200 mm×200 mm. The interior column was reinforced by 4-T13. However, the surrounding columns were reinforced by 8-T13 to further enhance their strength and stiffness. The drop panel was reinforced with a single layer mesh of R6@80 mm. The RC flat slab was reinforced using two layers of R6@250 mm mesh. Moreover, in the bottom layer, integrity rebar of 3R6 was installed within the column reinforcing cage in orthogonal directions, to meet the detailing requirements of ACI 381-11 [26] (more than two reinforcements passing through the column cage as integrity rebar). T13 and R6 represent the deformed rebar with diameter of 13 mm and plain rebar with diameter of 6 mm, respectively. The yield strength and ultimate strength of R6 were 500 MPa and 617 MPa, and those of T13 were 529 MPa and 608 MPa. After 28 days curing, the measured concrete compressive strength of Specimens ND and WD was 22.5 MPa and 22.3 MPa, respectively.

Test setup and instrumentation layout of Specimen WD are shown in Fig. 2. As shown in the figure, the specimen was supported by eight steel legs. A special load distribution rig was designed to equivalently replicate the uniform distributed load (UDL). The detailing of the load distributed rig is illustrated in Fig. 3. It has three rigid beams, four triangle steel plates, and twelve small steel plates. Between the secondary steel beams and triangle steel plates, hemisphere balls and socket joints were utilized to ensure the load can be vertically applied during the tests, even at the stage that the large deformation of slabs. Moreover, a hydraulic jack with a stroke of 600 mm was utilized to apply loads and a steel assembly (Item 4 in Figure 2) was designed to ensure that the applied load keeps vertically. More details about the test program please refer to Qian and Li [20].

2.2. Details of numerical model

In this study, high fidelity finite element model was developed to investigate the difference of load resisting mechanisms on each floor of a multi-storey flat slab structure subjected to a middle column removal scenario. The explicit software LS-DYNA [27] was employed due to its numerical stability and sufficient availability of constitutive models. Although quasi-static behavior of the flat slab substructure was focused on in this study, explicit solver was adopted to avoid divergence problem at large deformation stage.

2.2.1 Element type

Fig. 4 shows the geometrical model of WD. For another model ND, it is identical to WD in slabs, columns, and reinforcement details, except no drop panels are modelled. To simulate the boundary conditions more close to real test conditions, eight steel legs and the load distribution rig were also simulated in FE modeling. The element of concrete adopted in this study is 8-node solid elements with reduced integration. This reduced integration element can save computational time on the premise of accuracy when hourglass control is well defined. To ensure the hourglass energy was less than 10 % of the total internal energy, Flanagan-Belytschko stiffness form with exact volume integration was used for solid elements. Thus, the hourglass coefficient was defined as 0.002. A 2-node Hughes-Liu beam element with 2×2 Gauss quadrature integration was employed to simulate the reinforcements. This Hughes-Liu beam element could effectively simulate the mechanical behavior of reinforcement bars, such as axial force, bi-axial bending, and transverse shear. Moreover, the load distribution rig and steel supports were also modeled by explicit solid element.

For the connection between reinforcement and concrete, previous studies [10, 14] had proved that the assumption of perfect bonding between slab reinforcement and concrete could ensure enough accuracy to simulate the behavior of RC component subjected to a column removal scenario. As a result, perfect bonding between concrete and reinforcement was assumed by keyword *Constrained_Lagrange_In_Solid in this study.

2.2.2 Boundary conditions and loading method

The RC slab was fixed onto the steel legs with shared nodes in the interface, as shown in Fig. 4. To ensure the beam elements and the concrete elements work together, the nodes at the end of longitudinal reinforcements of RC columns were tied to the steel plates by using keyword *Contact_Tied_Nodes_To_Surface. Fixed boundary conditions were applied at the bottom of the steel supports. Moreover, eight steel plates were modeled to apply the steel weights (Item 7 in Figure 2) as used in the reference test [20], as shown in Fig. 4. Steel plates were fixed to RC slab with contact surface using keyword ∗Contact_Automatic_Surface_To_Surface (*CASTS).

As shown in Fig. 5, the load distribution rig from Qian and Li [20] is simulated with high fidelity. It contains a series of rigid beams and plates. The top rigid beams were connected with the secondary rigid beam by revolute joints defined by keyword *Constrained_Joint_Revolute. The secondary rigid beam was connected with the triangle rigid plates by spherical joints defined by keyword *Constrained_Joint_Spherical. Revolute joints were defined between bottom small steel plates and the triangle steel plates to ensure the small plates were able to rotate around the revolute joints. Furthermore, single surface (*Contact_Automatic_Single_Surface) was defined between the load distribution rig and RC slab.

As shown in Fig. 5, a rigid plate with only vertical freedom was built on the middle of the first rigid beam to apply load on the slab. *CASTS were defined between the bottom surface of the rigid plate and the top surface of the first rigid beam. The vertical load from the hydraulic jack in the test program [20] was simulated by applying a velocity-time history for the rigid plate on the middle of the first rigid beam. The velocity increases from 0 mm/ms under a small constant acceleration at the beginning to avoid severe vibration of structural resistance, as suggested by the works [10, 28], and then stays constant. The maximum velocity and acceleration were set to 0.2 mm/ms and 6.7×10^{-4} mm/ms^2, respectively, by a sensitivity analysis based on Specimen ND.

2.2.3 Material model

In this study, continuous surface cap model (CSCM) was chosen to simulate the concrete properties, as several studies have proven its accuracy to simulate quasi-static behavior of RC components subjected to column removal scenarios [10, 14, 28, 29]. The CSCM can effectively simulate the material properties of concrete (such as damage–based softening and modulus reduction, shear dilation, shear compaction, confinement effect, and strain rate effect, etc.) under low confinement situations [30]. Its yield surface consists of shear failure surface and hardening cap surface [27], as shown in Fig. 6. The original CSCM (*Mat_CSCM) requires a series of input parameters to define concrete material properties. LS-DYNA also provides a simplified CSCM (*Mat_CSCM_CONCRETE) for concrete properties with unconfined compressive strength between 28 MPa and 48 MPa. The simplified CSCM only needs three input parameters (unconfined compressive strength f_c, maximum aggregate size A_g, and units), and then the remaining material properties are calculated automatically according to equations proposed by CEB-FIP concrete model code [31]. The unconfined compressive strength $f_c^{'}$ of Specimens ND and WD was 22.5 MPa and 22.3 MPa, respectively. For simplicity, the average value 22.4 MPa was applied in the numerical models. The maximum aggregate size A_g is 10 mm. However, the default concrete material properties would over-predict the structural resistances of FE models. Therefore, concrete material properties were made a few adjustments on the fracture energy. Previous studies [10, 28] suggest that the tensile fracture energy G_{ft} could take 80 % of the default one when it is over-prediction, and the shear fracture energy G_{fs} should be reduced as G_{fs} =50G_{ft} (The default is G_{fs} =100G_{ft}) when shear damage is evident. Both G_{ft} and G_{fs} are adjusted, as severe punching shear failure occurred in Specimen ND. The detailed parameters of CSCM are tabulated in Table 2. The unconfined uniaxial stress-strain relationship of concrete after adjustments is shown in Fig. 7. The CSCM also provides an erosion algorithm based on maximum principal strain to simulate material failure. If the maximum principal strain of concrete element is greater than the failure principal strain the concrete element will be deleted. Although element erosion has little physical meaning, several studies [10, 14, 28, 29] found that erosion criterion based on the maximum principal strain is a suitable way to simulate concrete failure under quasi-static condition. However, it will be very hard to simulate the shear failure of concrete if only the maximum principal strain criterion was used to define the erosion of concrete element. Thus, the maximum principal strain and shear strain criterions were taken into consideration in this study by using keyword *Mat_Add_Erosion. Since the appropriate values are dependent on mesh size, the values of principal strain and shear strain at failure were final set to 0.1 and 0.08, respectively, by many times of trial calculation based on Specimen ND. Furthermore, the strain rate effect was ignored since only quasi-static behavior was discussed in this study.

The isotropic elastic-plastic material model (*Mat_Plastic_Kinematic) was chosen for reinforcement. The parameters of material properties, including elastic modulus, yield strength, tangential modulus, and ultimate strain, were determined in accordance with the material tests. In addition, the strain rate effect was also ignored.

Sensitivity analysis was conducted with three mesh sizes, as listed in Table 3. As shown in Fig. 8, Mesh 2 is reasonable for Specimen ND, as further mesh refinement cannot lead to any remarkable convergence but instead taking more computing time. Therefore, the mesh size of concrete element was 18.33 mm×25 mm×25 mm for RC slab and 25 mm×25 mm×25 mm for other components. The size of beam element was 30 mm.

2.3 Validation by test results

Fig. 9 shows the comparison of load-displacement curves from FE simulation and experimental tests. For Specimen ND, as shown in Fig. 9(a), after reaching the yield load, the load resistance decreased due to secondary punching shear failure, which agrees with the experimental observation well. For Specimen WD, as shown in Fig. 9(b), the load resistance decreased slowly after reaching the first peak load (FPL), indicating its failure was mainly controlled by flexural failure, which was similar to that of test results. The error of key results between the FE models and test specimens is less than 10 %, as listed in Table 4. Therefore, the proposed FE models could effectively simulate the behavior of punching shear failure and the effectiveness of drop panels.

It should be noted that the concrete damage was expressed by the damage index. Damage index of 0 and 1 represents no damage and completed failure, respectively. As shown in Figs. 10 and 11, FE model could simulate the crack pattern of tested specimen well. For Specimen ND, FE model could predict the punching shear failure of the slab-column connection well, as shown in Fig. 12. As shown in Fig. 13, the failure mode of Specimen WD could also be well simulated. As a result, the FE models could be used for further parametric study.

3. Effects of boundary condition simplification

For both specimens, due to the limitation of cost and space, only substructures (two-bay by two-bay) were tested. However, in reality, the remaining parts of the building (such as the surrounding slabs and upper floors) may affect the response of the substructures significantly, which was ignored in experimental program. As a result, in this section, the validated FE models were utilized to quantify the effects of boundary condition simplification.

3.1. Effects of surrounding slabs

Around the substructure, the surrounding slabs will provide certain constraints (rotational, horizontal, or vertical constraints). However, for Specimens WD and ND, the constraints from surrounding slabs were simulated by applying service pressure at the overhang, which is one-quarter of column spacing. Previous works [25] found that the simplified boundary may underestimate the constraints from surrounding slabs. Thus, to further understand the discrepancy between the simplified boundaries and realistic boundaries, four numerical models with different constraints at the overhang (refer to Fig. 14) and one numerical model with four-bay by four-bay (refer to Fig. 15) were developed based on the validated FE model for Specimen ND. As shown in Fig. 14, ND-P, ND-H, ND-V, and ND-F represent ND with design gravity loads (live and dead) at the overhang, with rigid horizontal constraint applied at the overhang edge, with rigid vertical constraint applied at the overhang edge, full constraints (rotational, horizontal, and vertical constraints) applied at the overhang edge, respectively. It should be noted that the design gravity load (live and dead) was also applied at the overhang of ND-H, ND-V, and ND-F. Moreover, as shown in Fig. 15, ND-R was modelled in four-bay by four-bay to include the effects of surrounding slabs realistically. Similarly, for ND-R, the design gravity load (live and dead) was also applied at the surrounding slabs.

Fig. 16 compares the load-displacement curves of ND with varying constraints. The load resistances of ND-P and ND-V are exactly same but lower than that of ND-R, indicating that the simplified boundary condition for tested specimens underestimates the constraints from surrounding bay. In addition, the rigid vertical constraint at the overhang edge has little effects on the load resistance. Conversely, ND-F with full constraints at the overhang edge (model ND-F) achieves higher load resistance than that of ND-R. Similar conclusion was obtained by Peng et al. [32]. However, the load resistance of model ND-H is very close to that of ND-R. The comparison of ND-H and ND-F indicates that the rotational restraint at the overhang edge could further increase the load resistance. Thus, to achieve more realistic structural response, only rigid horizontal constraints should be applied at the slab edge.

3.2. Effects of upper floors

Only single-story flat slab substructures were tested in the test program [20]. However, progressive collapse is a global behavior. Thus, it is necessary to investigate the response of multi-story flat slab structure. As shown in Fig.17, ND-1F, ND-2F, and ND-3F represent single-story, two-story, and three-story flat slab substructure, respectively. The dimension, reinforcement details, and boundary conditions at the overhang edge in each story are identical as those at model ND. The load distribution rig was generated in each story, and identical service load was applied at the overhangs of each story.

To be consistent, it should be noted that only the load resistance from the first story of these models was extracted for comparison, as shown in Fig. 18. It can be seen that the load resistance of ND-2F is extremely similar to that of ND-1F. Although ND-3F achieved largest load resistance before occurrence of the secondary punching shear failure, the maximum difference is less than 5 %. As a result, the structural response of the extracted substructure is insensitive to the constraints from the upper stories.

3.3. Combined effects due to surrounding slabs and upper floors

To investigate the combined effect due to surrounding slabs and upper floors, a global FE model ND-3F-R was built based on ND-3F, as shown in Fig. 19. ND-3F-R (four-bay by four-bay but three stories) has similar reinforcement details and dimensions as ND-3F and surrounding slabs were also modelled directly. Design gravity loads (live and dead) were also applied on the surrounding slabs.

Fig. 20 shows the comparison of the resistances of the first story between ND-1F and ND-3F-R. As can be seen in the figure, the FPL of ND-3F-R is larger than that of ND-1F by 13.8 %. Note that the FPL of ND-R is larger than that of ND-P by 12.6 % (effect of surrounding slabs while the FPL of ND-3F is larger than that of ND-1F by 1.0 % (effect of upper floors). Therefore, the effects of surrounding slabs and upper floors could be superposed.

4. Load resisting mechanisms of each story for a multi-storey flat slab structure

As aforementioned, progressive collapse is a global behavior for a multi-storey building. However, majority of existing tests in progressive collapse investigation were based on single-storey substructures due to cost and time limitation. These studies are based on the assumption that each story of the structures has identical load resistance and load resisting mechanisms at same deformation stages. However, in reality, above assumption is not true even all floors above the lost column have identical structural components. To evaluate the accuracy of above assumption, the structural response of each story was extracted for comparison based on the models of ND-2F, ND-3F, and ND-3F-R.

For ND-2F and ND-3F, as shown in Figs. 21(a) and (b), the structural resistance developing in each story is different. The maximum resistance is observed in the first story. It could be explained that the interaction among different stories, which leads to different in-plane force developed in slab within different stories and mobilization of membrane actions (CMA and TMA). To elaborate on this assumption, the in-plane forces of the slab sections in x direction, as labeled in Fig. 22, were extracted to elucidate the membrane actions developing in flat slab substructure. For simplicity, only the section force of ND-3F was presented. As shown in Fig. 23, the development of the slab-section force in each story is different. In the first story, the section force developing in the slab is in compression (negative) firstly, and then transfers into tension at the large deformation stage. However, the section force of the second story or the third story is always in tension or in compression, respectively. Moreover, the peak value of the section force in the first story is much larger than the ones of other stories. Therefore, for ND-2F and ND-3F, CAA and TMA could develop in the first story effectively, leading to larger resistance. For ND-3F-R, which has a close-to-reality boundary condition, the structural resistance developing in each story is also different. As shown in Fig. 21(c), when the vertical displacement of the middle column is less than 88 mm, the load resistance of the first story is larger than that from the second and third stories.

5. Parametric study

To deeply understand the behavior of flat slab structures to resist progressive collapse, a parametric study was also performed based on the validated FE models.

5.1. Effects of integrity reinforcement

As mentioned above, in the reference tests [20], 3R6 integrity reinforcements were designed passing through the column cages in each principal direction, which was greater than that suggested by ACI 318-11 (2011) [26]. Nevertheless, there was no specific calculation formula for designing of the integrity reinforcement. The arrangement of the integrity reinforcement may affect the load resisting capacity after punching shear failure and deformation capacity of the flat slab structure. Thus, in this section, to quantify the effects of the amount of integrity reinforcement, FE models with different amounts of integrity reinforcement were simulated. Seven different cases (including 0, 1R6, 2R6, 3R6, 4R6, 5R6, and 6R6 integrity reinforcements) were considered for ND. Moreover, four different cases (including 0, 1R6, 2R6, and 3R6 integrity reinforcements) were considered for ND-R to investigate the effects of integrity reinforcement under a more real boundary condition. To normalize the amount of integrity reinforcement, integrity reinforcement ratio $\rho_i = A_s/bh_o$ is used. A_s is the total area of the integrity reinforcements; b is the column width (200 mm for these specimens); and h_o is the effective depth of the slab (45 mm for these specimens). Thus, ρ_i of 1R6, 2R6, 3R6, 4R6, 5R6 and 6R6 are 0.31 %, 0.63 %, 0.94 %, 1.26 %, 1.57 %, and 1.88 %, respectively.

Fig. 24 shows the load-displacement curves of ND with the different amount of integrity reinforcement. The key results are listed in Table 5. As can be seen in the figures and table, with the increase of integrity reinforcement ratio from 0 % to 1.88 % (0 to 6R6), the YL, FPL, and second peak load (SPL) increased by 18.5 %, 41.6 %, and 209.4 %, respectively. It is obvious that increasing the integrity reinforcement ratio can enhance the load resisting capacity at large deformation stage after column removal significantly. This is mainly due to the enhancement of dowel action from integrity reinforcement. However, the efficiency of upgrading the load resisting capacity decreases with increasing the amount of integrity reinforcements. For instance, the YL increases by 15.9 % when the integrity reinforcement ratio increases to 0.94 % (3R6). However, when the integrity reinforcement ratio increases to 1.88 % (6R6), the YL only increases by 18.5 %. Similar phenomenon is observed for the FPL. It is found that when the integrity reinforcement ratio of ND is greater than 0.63 % (2R6), the SPL exceeds the FPL. In summary, to have a good post-punching performance of the flat slab structure subjected to the loss of a middle column scenario, the integrity reinforcement ratio is suggested to greater than 0.63 %.

Comparing to ND, ND-R may be more prone to failure since extra load from surrounding slabs transfers to the adjacent slab-column connections. As shown in Fig. 25, when there is no integrity reinforcement installed passing through the column cages, the structural resistance of ND-R drops to 0 kN suddenly after the secondary punching shear failure occurred. This is because when punching shear failure occurred at one of adjacent slab-column connections, it started to propagate horizontally due to further load redistribution and resulted in total collapse of entire slab, as shown in Fig. 26. Moreover, similar to ND, it can be found that installing 2R6 (ρ_i=0.63 %) integrity reinforcements in ND-R can ensure that the SPL (180.2 kN) exceeds the FPL (178.5 kN).

5.2. Effects of slab thickness

Previous work [19] investigated different slab thickness of RC flat slab structures subjected to the loss of a middle column scenario. However, their specimens were tested under concentrated load. To re-evaluate the effects of slab thickness of RC flat slabs subjected to the loss of a middle column under UDL loading regime, models with slab thickness of 70 mm and 100 mm were simulated based on the validated FE models ND and WD. These models are the same as the validated FE models except the slab thickness.

Figs. 27(a) and (b) show the load-displacement curves of WD and ND with different slab thicknesses, respectively. To distinguish, WD with slab thickness of 55 mm, 70 mm, and 100 mm are named WD-55, WD-70, and WD-100, respectively. Similarly, ND-55, ND-70 and ND-100 represent ND with slab thickness of 55 mm, 70 mm, and 100 mm, respectively. As shown in Fig. 27(a), a thicker slab could increase the load resisting capacity significantly. The FPL of WD-100 is larger than that of WD-70 and WD-55 by 65.8 % and 177.1 %, respectively, which is different from the concentrated loading regime in [19]. For WD-70 and WD-100, no obvious re-ascending of load resistance is observed at the large deformation stage after column removal. This is because the residual load-resisting capacity at the large deformation stage is mainly provided by the dowel action from integrity reinforcements and TMA developed in remaining bottom slab reinforcements. However, increasing the slab thickness has little effects on the development of these actions. Moreover, by comparing Fig. 13 with Fig. 28, it is found that the failure modes of WD-100 and WD-70 are quite different to that of WD-55. The main cracks of WD-100 and WD-70 are formed at the edge of column while those of WD-55 are formed at the edge of drop panels, indicating that the drop panels of WD-100 and WD-70 lose its efficiency for preventing punching shear failure at slab-column connections. Therefore, the thickness of drop panel should be increased proportionately with the increase of the slab thickness to ensure its efficiency.

For ND-series, similar to WD-series, specimen with a thicker slab has a greater FPL and lower deformation capacity, as shown in Fig. 27(b). The FPL of ND-100 is larger than that of ND-70 and ND-50 by 84.0 % and 197.8 %. Moreover, punching shear failure was observed in ND-100 before reaching its yield load. Conversely, punching shear failure was observed after reaching their yield load for ND-70 and ND-55, which indicates that the failure mode prone to brittle punching shear failure with increasing the slab thickness.

6. Conclusions

Following conclusions can be made through the studies presented in this paper:

1. The numerical models built by LS-DYNA are able to simulate the structural behavior of RC flat slab substructures subjected to a middle column missing scenario under quasi-static loading regime well. The CSCM employed in the model can effectively predict the punching shear failure at slab-column connections.
2. Numerical analysis on different boundary conditions at the overhang edge indicates that using fixed constraints at the slab edges may over-estimate the response, while only rigid horizontal constraints at the overhang edge are more realistic.
3. The numerical results indicated in numerical or experimental studies, only considering first storey or including upper stories does not alter the response of the first floor greatly. However, the load resistance from each story in a multi-storey building is different. This is because the interaction among the stories causes different in-plane force developed in each story, which influences the mobilization of membrane actions (CMA and TMA).
4. Increasing the integrity reinforcement ratio can increase the yield load, first peak load, and second peak load of the specimens, especially for second peak load. The numerical results indicate that the minimum integrity reinforcement ratio is suggested to be 0.63 % to ensure good post-punching performance of the flat slab substructure to resist progressive collapse.

5. For RC flat slab structure under uniformly distributed load condition increasing the slab thickness could significantly increase the first peak load while reduce the deformation capacity remarkable. This is because the slab thickness has little effects on the residual load resisting capacity at large deformation stage after column removal.

7. Acknowledgements

This research was supported by a research grant provided by the Natural Science Foundation of China (Nos.51778153, 51568004, 51478118). Any opinions, findings and conclusions expressed in this paper do not necessarily reflect the view of Natural Science Foundation of China.

References

[1] Department of Defense (DoD). Design of building to resist progressive collapse. Unified Facility Criteria, UFC 4-023-03. Washington (DC): US Department of Defense, 2009.

[2] GSA. Progressive collapse analysis and design guidelines for new federal office buildings and major modernization projects. U.S. General Service Administration, 2003, Washington, DC.

[3] ASCE/SEI 7. Recommendations for designing collapse-resistant structures. Structural Engineering Institute-American Society of Civil Engineers, 2010, Reston, VA.

[4] COST Action TU0601. Robustness of structures. Proceedings of the 1st Workshop. ETH Zurich: European Cooperation in Science and Technology, 2008.

[5] Y.P. Su, Y. Tian, X.S. Song, Progressive collapse resistance of axially-restrained frame beams, ACI Struct. J. 106(5) (2009) 600-607.

[6] J. Yu, K.H. Tan, Experimental and numerical investigation on progressive collapse resistance of reinforced concrete beam column sub-assemblages, Eng. Struct. 55 (2013) 90-106.

[7] D.C. Feng, Z. Wang, G. Wu, Progressive collapse performance analysis of precast reinforced concrete structures, Struct. Design Tall Spec. Build. 28 (2019).

[8] A. Fascetti, S.K. Kunnath, N. Nistico, Robustness evaluation of RC frame buildings to progressive collapse, Eng. Struct. 86 (2015) 242-249.

[9] E. Livingston, M. Sasani, M. Bazan, S. Sagiroglu, Progressive collapse resistance of RC beams, Eng. Struct. 95 (2015) 61-70.

[10] J. Yu, L.Z. Luo, Y. Li, Numerical study of progressive collapse resistance of RC beam-slab substructures under perimeter column removal scenario, Eng. Struct. 159 (2018) 14-27.

[11] S.D. Shan, S. Li, S.Y. Xu, L.L. Xie, Experimental study on the progressive collapse performance of RC frames with infill walls, Eng. Struct. 111 (2016) 80-92.

[12] F. Sadek, J. Main, H. Lew, Y. Bao, Testing and analysis of steel and concrete beam-column assemblies under a column removal scenario, J. Struct. Eng. 137(9) (2011) 881-892.

[13] K. Qian, B. Li, Slab effects on response of reinforced concrete substructures after loss of corner column, ACI Struct. J. 109 (6) (2012) 845-855.

[14] A.T. Pham, N.S. Lim, K.H. Tan, Investigations of tensile membrane action in beam-slab systems under progressive collapse subject to different loading configurations and boundary conditions, Eng. Struct. 150 (2017) 520-536.

[15] X.Z. Lu, K.Q. Lin, Y. Li, H. Guan, P.Q. Ren, Y.L. Zhou, Experimental investigation of RC beam-slab substructures against progressive collapse subject to an edge-column-removal scenario, Eng. Struct. 149 (2017) 91-103.

[16] P.Q. Ren, Y. Li, X.Z. Lu, H. Guan, Y.L. Zhou, Experimental investigation of progressive collapse resistance of one-way reinforced concrete beam-slab substructures under a middle-column-removal scenario, Eng. Struct. 118 (2016) 28–40.

[17] D.C. Feng, S.C. Xie, W.N. Deng, Z.D. Ding, Probabilistic failure analysis of reinforced concrete beam-column sub-assemblage under column removal Scenario, Eng. Fail. Anal. 100 (2019) 381-392.

[18] J.M. Russell, J.S. Owen, I. Hajirasouliha, Experimental investigation on the dynamic response of RC flat slabs after a sudden column loss, Eng. Struct. 99 (2015) 28-41.

[19] K. Qian, B. Li, Resilience of flat slab structures in different phases of progressive collapse, ACI Struct. J. 113(3) (2015) 537-548.

[20] K. Qian, B. Li, Load-resisting mechanism to mitigate progressive collapse of flat slab structures, Mag. Concr. Res. 67(7) (2015) 349-363.

[21] F. H. Ma, B. P. Gilbert, H. Guan, H. Z. Xue, X. Z. Lu, Y. Li, Experimental study on the progressive collapse behavior of RC flat plate substructures subjected to corner column removal scenarios, Engineering Structures, 180 (2019) 728-741.

[22] L. Keyvani, M. Sasani, Y. Mirzaei, Compressive membrane action in progressive collapse resistance of RC flat plates, Eng. Struct. 59 (2014) 554-564.

[23] R.J. Liu, Y. Tian, S.L. Orton, A.M. Said, Resistance of flat-plate buildings against progressive collapse. I: modeling of slab-column connections, J. Struct. Eng. 141(12) (2014) 04015053.

[24] Z.H. Peng, S.L. Orton, J.R. Liu, Y. Tian, Experimental study of dynamic progressive collapse in flat-plate buildings subjected to exterior column removal, J. Struct. Eng. 143(9) (2017) 04017125.

[25] K. Qian, Y.H. Weng, B. Li, Impact of two columns missing on dynamic response of RC flat slab structures, Eng. Struct. 177 (2018) 598-615.

[26] ACI Committee 318. Building code requirements for structural concrete (ACI 318-11) and commentary (318R-11). American Concrete Institute, 2011, Farmington Hills, MI, p. 433.

[27] J. Hallquist, LS-DYNA keyword user's manual, Version 971, Livermore Software Technology Corp., 2007, Livermore, CA.

[28] J. Yu, Y.P. Gan, J. Wu, H. Wu, Effect of concrete masonry infill walls on progressive collapse performance of reinforced concrete infilled frames, Eng. Struct. 191 (2019) 179-193.

[29] A.T. Pham, K.H. Tan, J. Yu, Numerical investigations on static and dynamic responses of reinforced concrete sub-assemblages under progressive collapse, Eng. Struct. 149 (2017) 2-20.

[30] Y. Wu, J.E. Crawford, J.M. Magallanes, Performance of LS-DYNA concrete constitutive models, 12th Int. LS-DYNA Users Conf., Livermore Software Technology Corporation, 2012, Livermore, CA.

[31] CEB. CEB-FIP model code 1990. 1991, Thomas Telford.

[32] Z.H. Peng, S.L. Orton, J.R. Liu, Y. Tian, Effects of in-plane restraint on progression of collapse in flat-plate structures, Journal of Performance of Constructed Facilities. 31(3) (2017) 04016112.

Figure caption list

Fig. 1. Dimension and reinforcement details of Specimen WD (unit: in mm)

Fig. 2. An overview of a specimen in position ready for testing

Fig. 3. The detailing of load distribution rig (Item 9 in Figure 2)

Fig. 4. Numerical model of Specimen WD

Fig. 5. Details of numerical model for load distribution rig

Fig. 6. Yield surface of CSCM model

Fig. 7. Unconfined uniaxial stress-strain relationship of concrete based on CSCM model

Fig. 8. Comparison of different mesh sizes

Fig. 9. Comparison of the load-displacement curves between simulation and test

Fig. 10. Comparison of crack pattern of ND from simulation and test

Fig. 11. Comparison of crack pattern of WD from simulation and test

Fig. 12. Failure mode of ND

Fig. 13. Failure mode of WD

Fig. 14. Different constrains of overhang edge

Fig. 15. Numerical model of ND-R

Fig. 16. Comparison of load-displacement curve of ND with varying constraints

Fig. 17. Numerical models of multi-story RC flat slab substructures

Fig. 18. Comparison of resistance in the first story of the multi-story RC flat slab substructures

Fig. 19. Numerical models of ND-3F-R

Fig. 20. Comparison of the load resistance of the first story from ND-1F and ND-3F-R

Fig. 21. Comparison of the load resistance from different stories

Fig. 22. Locations of slab sections

Fig. 23. Comparison of the in-plane force in x direction

Fig. 24. Comparison of ND with different number of integrity reinforcements

Fig. 25. Comparison of ND-R with different number of integrity reinforcements

Fig. 26. Failure mode of ND-R without integrity reinforcement

Fig. 27. Investigation on effects of slab thickness

Fig. 28. Failure modes of WD-70 and WD-100

Table 1. Specimen properties from Qian and Li [20]

Test	Elements				Slab Rebar		
	Interior Column stub	Edge or Corner Columns	Drop Panel Thickness	Drop Panel Rebar, mm	Slab Thickness	Top Layer, mm	Bottom Layer, mm
ND	Height=390 mm Cross-section= 200×200 mm^2 Reinforcement ratio=1.3%	Height=300 mm Cross-section= 200×200 mm^2 Reinforcement ratio=2.6%	N.A	N.A	55 mm	R6@250	R6@250
WD			35 mm	R6@80	55 mm	R6@250	R6@250

Table 2. User-input parameters of CSCM (Units: N, mm and ms)

MID	RO	NPLOT	INCRE	IRATE	ERODE	RECOV	ITRETRC
1	0.00232	1	0.0	0	1.10	0.0	0
PRED							
0							
G	K	ALPHA	THETA	LAMDA	BETA	NH	CH
10396.30	11386.43	13.2996	0.2734	10.5	0.01929	0	0
ALPHA1	THETA1	LAMDA1	BETA1	ALPHA2	THETA2	LAMDA2	BETA2
0.74735	0.001327	0.17	0.07680	0.66	0.001596	0.16	0.07680
R	XD	W	D1	D2			
5.0	87.6	0.05	2.5e-04	3.492e-07			
B	GFC	D	GFT	GFS	PWRC	PWRT	PMOD
100.0	3.7760	0.1	0.03776	0.01888	5.0	1.0	0.0
ETA0C	NC	ETAOT	NT	OVERC	OVERT	SRATE	REPOW
0	0	0	0	0	0	0	0

Table 3. Sensitivity analysis on mesh size

Type	Mesh 1	Mesh 2	Mesh 3
Mesh size at flat slab (mm)	30 × 30 × 27.5	25 × 25 × 18.33	15 × 15 × 13.75
Mesh size at other parts (mm)	30 × 30 × 30	25 × 25 × 25	15 × 15 × 15
Length of beam element (mm)	30	30	15
Total number of solid elements	63,891	104,784	392,800
Total number of beam elements	9386	9386	21,550
Computing time (s)	8912	12,152	29,250

Table 4. Comparison of the key results between test specimens and FE models

Results Source	ND			WD		
	YL (kN)	FPL (kN)	ULC (kN)	YL (kN)	FPL (kN)	ULC (kN)
Test	134.3	180.8	206.3	185.6	241.5	251.3
FE	137.4	179.5	209.2	190.5	238.6	235.4
FE/Test	1.02	0.99	1.01	1.03	0.99	0.94

Note: YL represents yield load; FPL represents first peak load; ULC represents ultimate load capacity.

Table 5. Key results of ND with different amount of integrity reinforcement

Amount (ρ_i %)	YL kN	FPL kN	SPL kN	Disp. of SPL mm
None	118.5	147.9	82.3	104.1
1R6 (0.31)	122.6	154.6	123.9	164.1
2R6 (0.63)	126.8	171.7	179.8	154.0
3R6 (0.94)	137.4	179.5	209.2	140.4
4R6 (1.26)	138.2	191.7	224.1	139.9
5R6 (1.57)	138.8	196.9	240.3	123.2
6R6 (1.88)	140.4	209.4	254.6	115.3

Note: YL represents yield load; FPL represents first peak load; SPL represents second peak load.

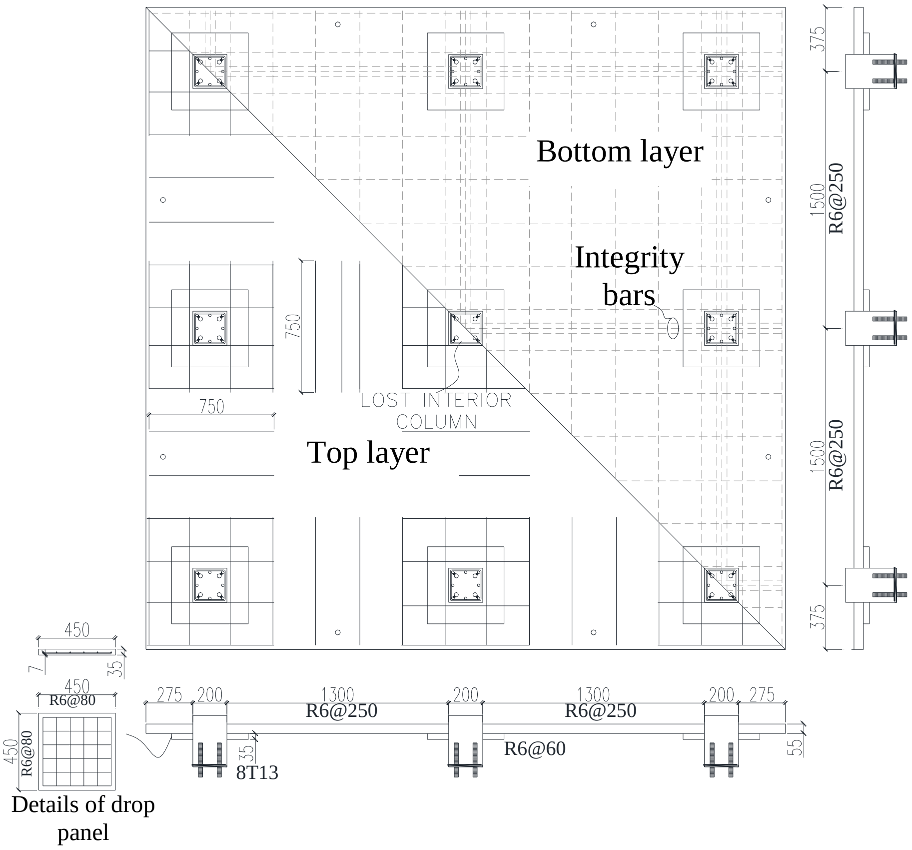

Fig. 1. Dimension and reinforcement details of Specimen WD (unit: in mm)

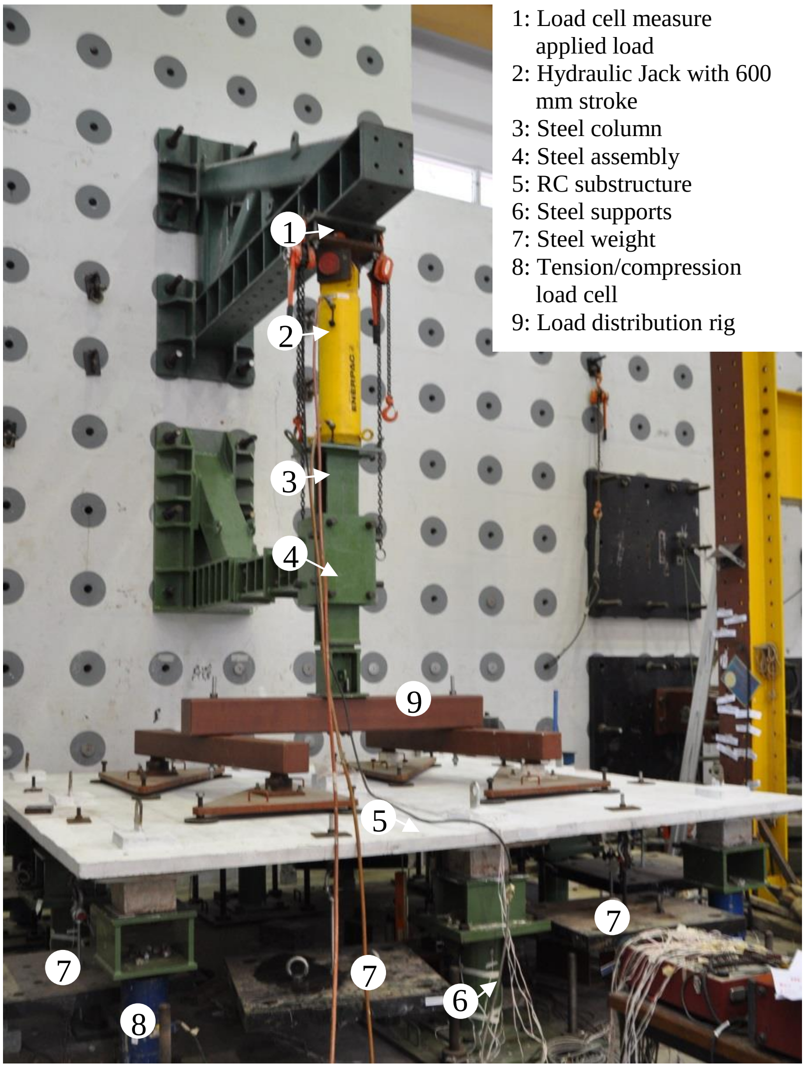

Fig. 2. An overview of a specimen in position ready for testing

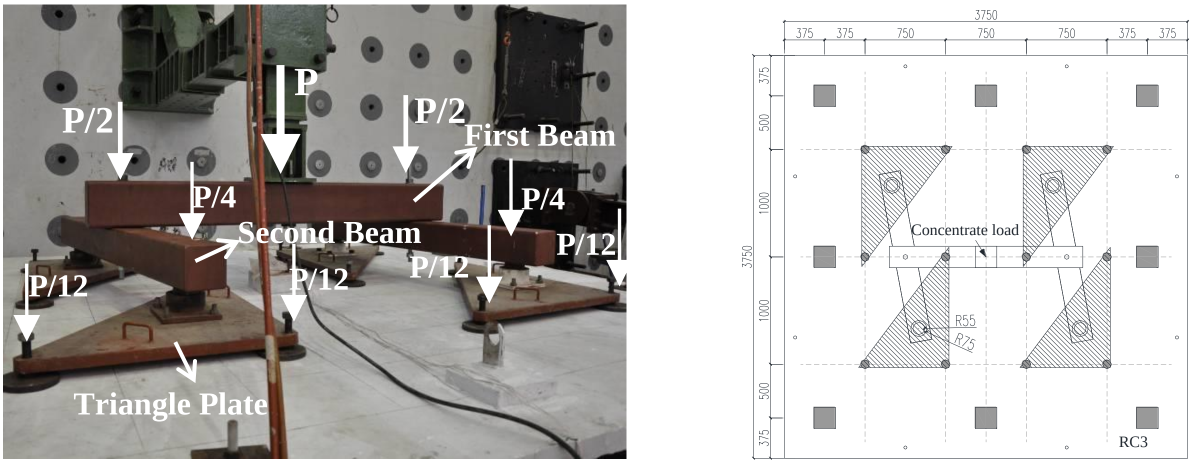

(a) Schematic of the load distribution (b) Arrangement of the twelve loading points

Fig. 3. The detailing of load distribution rig (Item 9 in Figure 2)

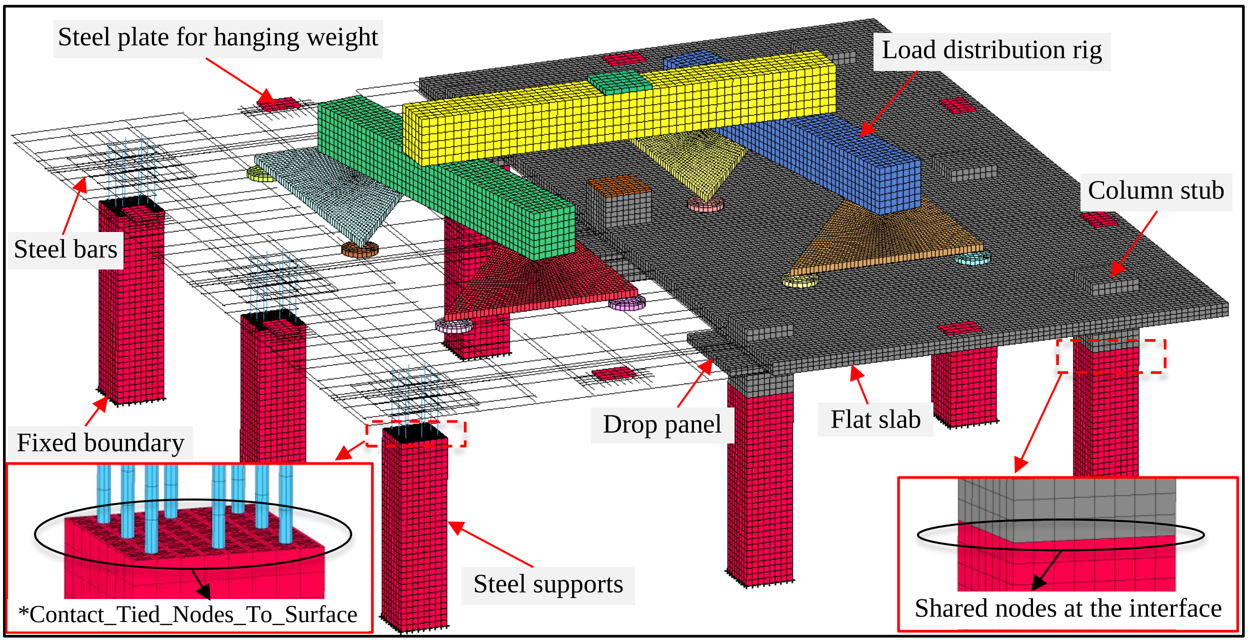

Fig. 4. Numerical model of Specimen WD

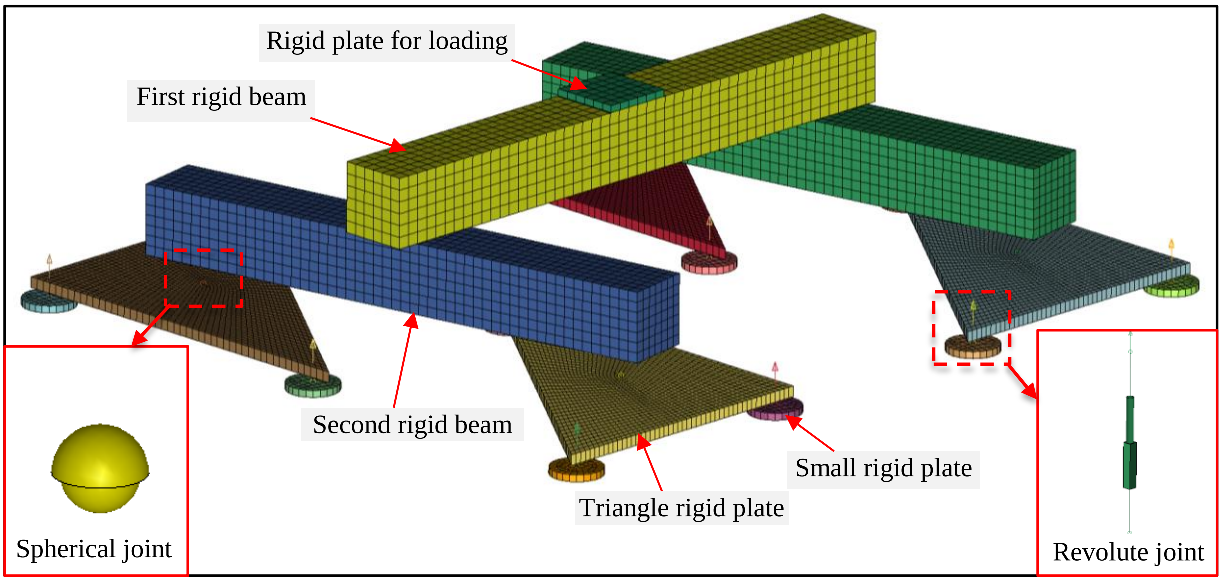

Fig. 5. Details of numerical model for load distribution rig

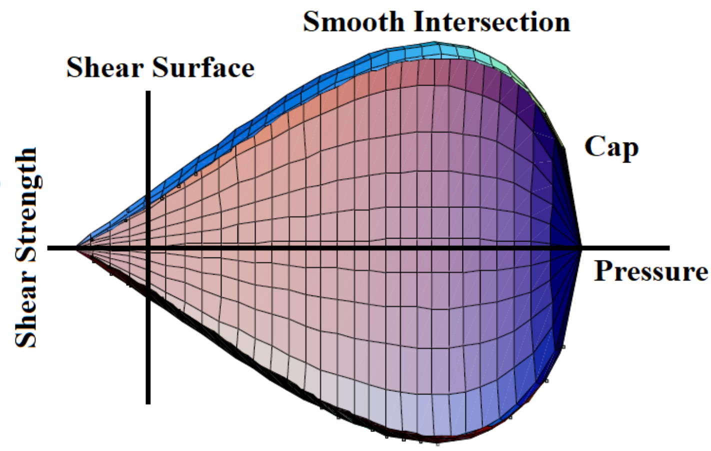

Fig. 6. Yield surface of CSCM model

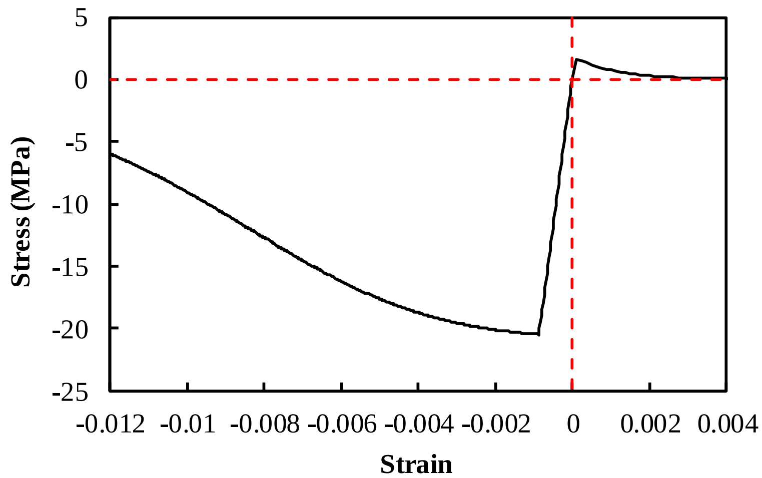

Fig. 7. Unconfined uniaxial stress-strain relationship of concrete based on CSCM model

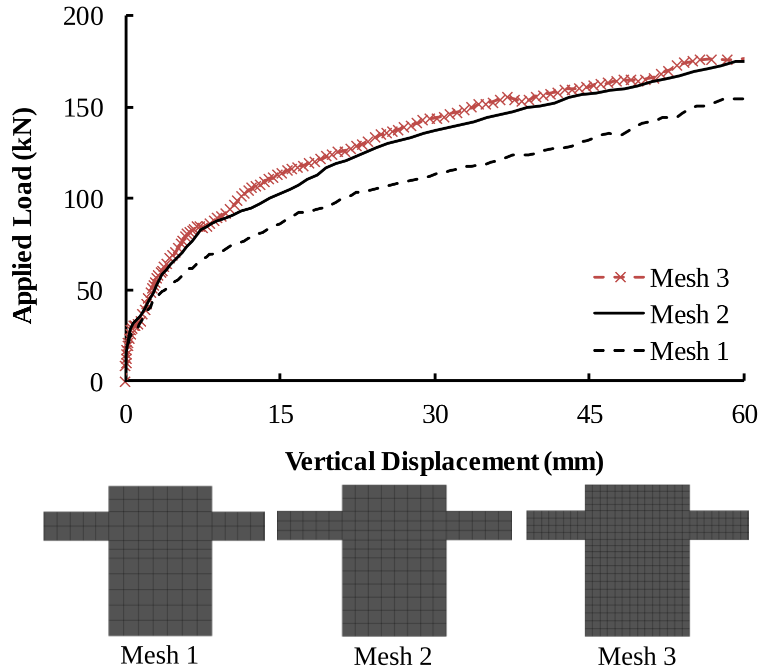

Fig. 8. Comparison of different mesh sizes

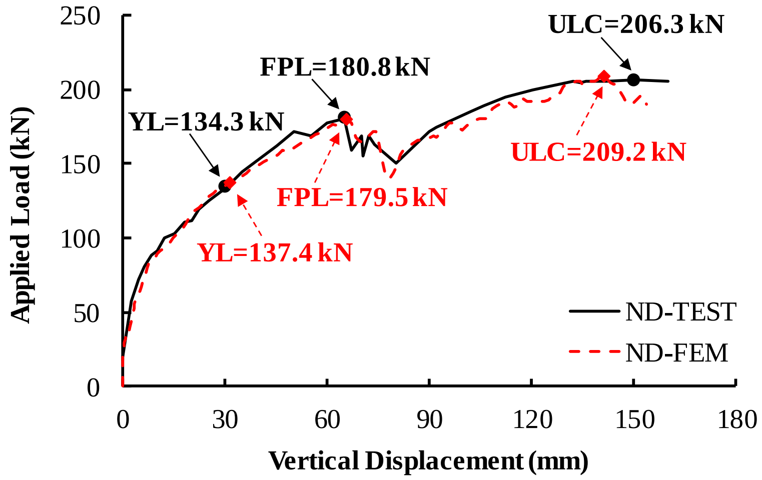

(a) ND

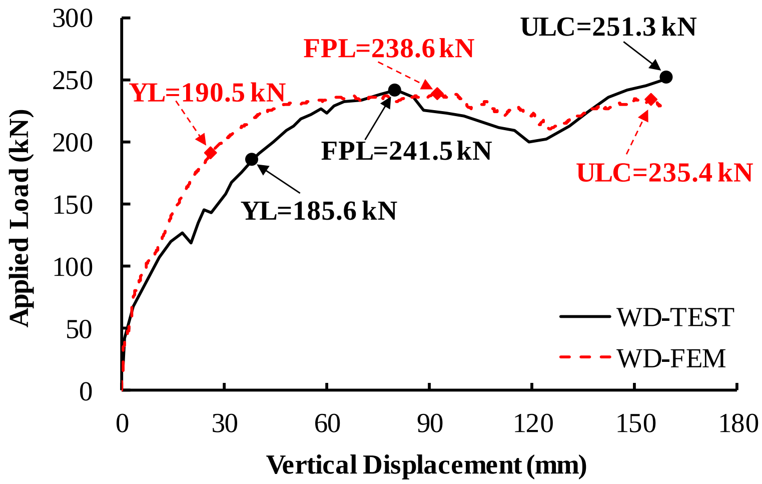

(b) WD

Fig. 9. Comparison of the load-displacement curves between simulation and test

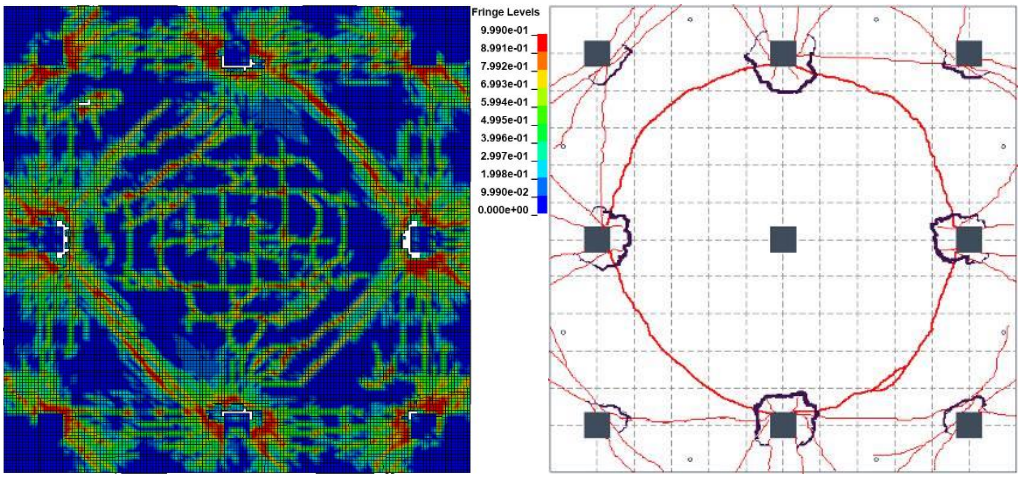

(a) Top view

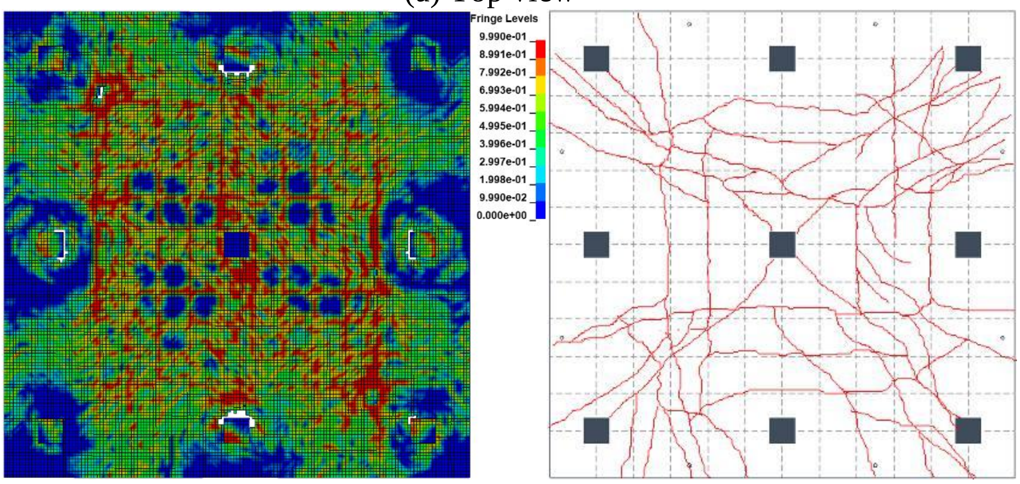

(b) Bottom view

Fig. 10. Comparison of crack pattern of ND from simulation and test

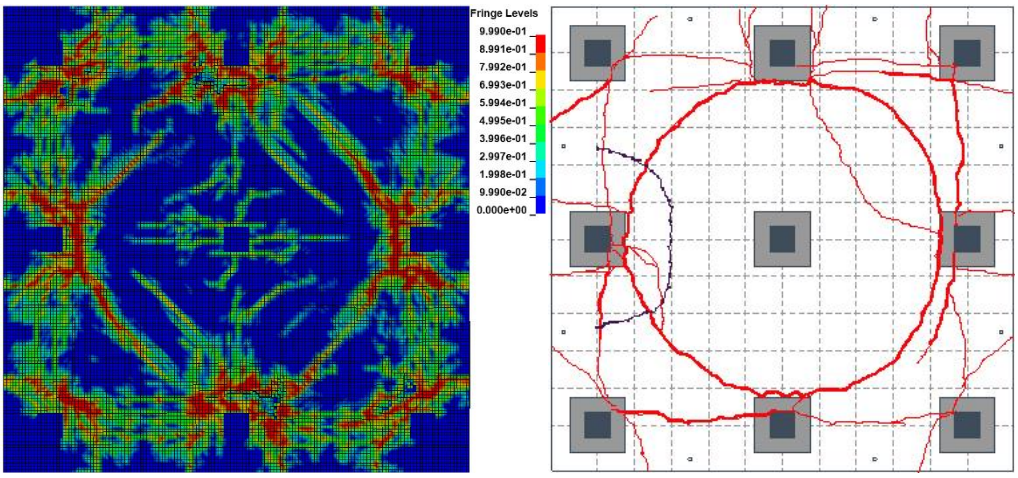

(a) Top view

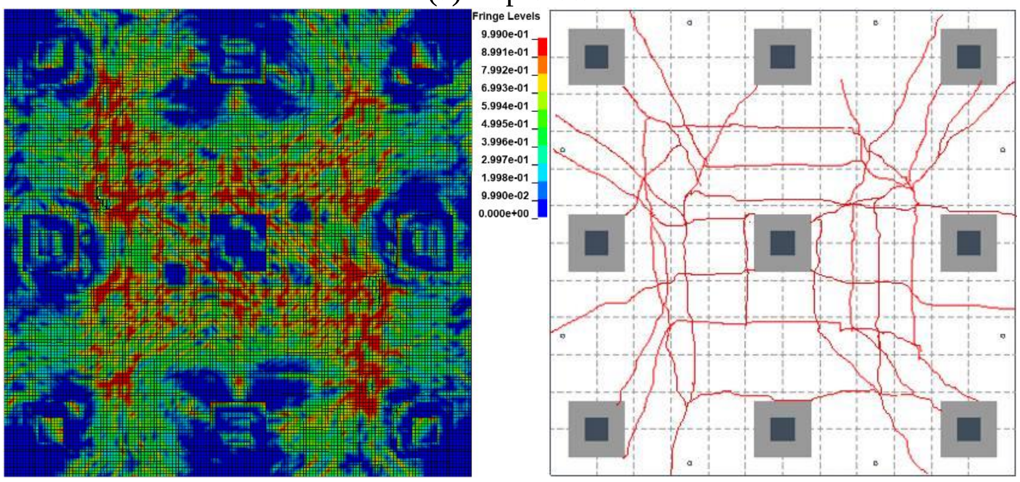

(b) Bottom view

Fig. 11. Comparison of crack pattern of WD from simulation and test

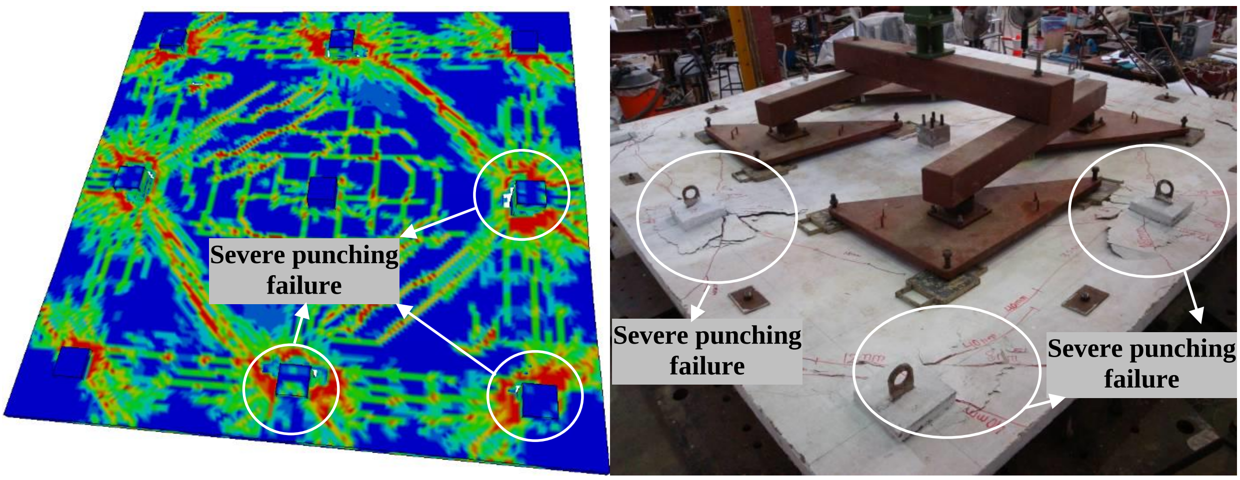

(a) FEM (b) Test [20]

Fig. 12. Failure mode of ND

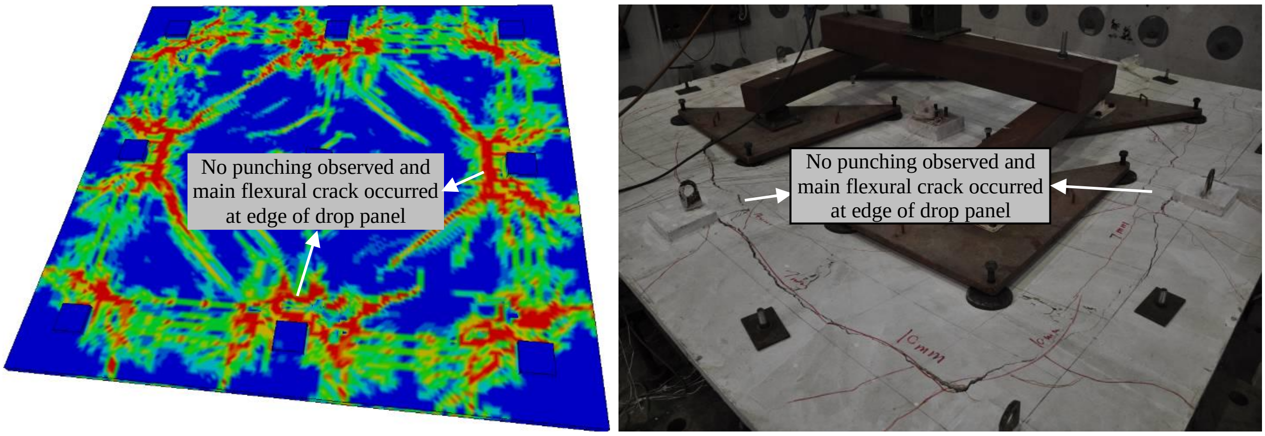

(a) FEM (b) Test [20]

Fig. 13. Failure mode of WD

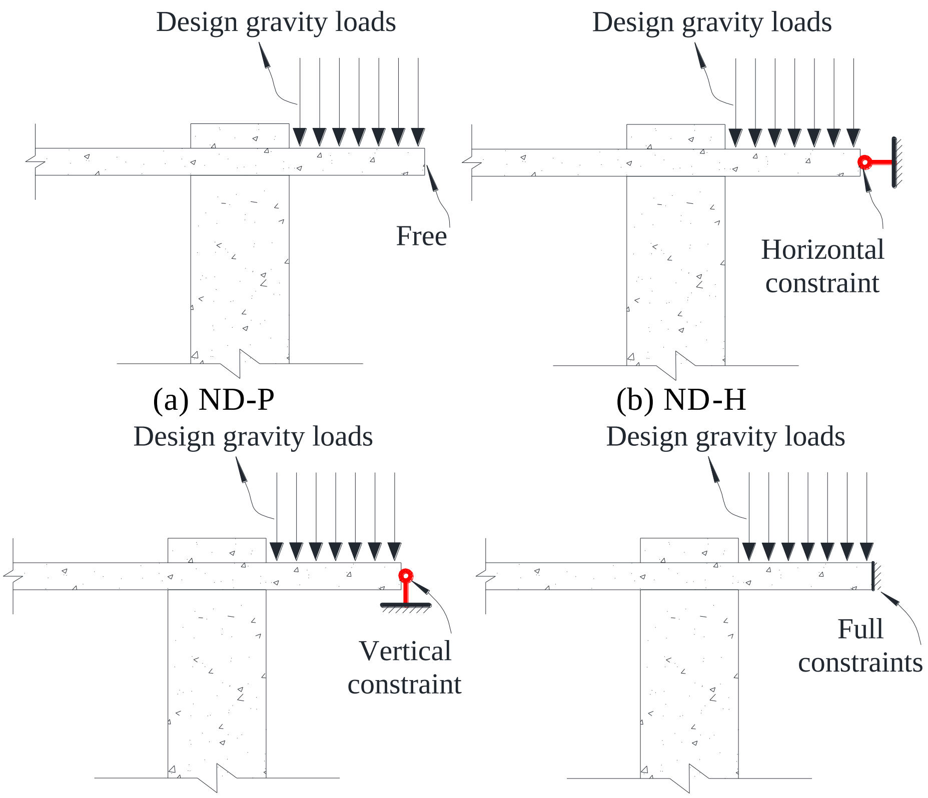

(c) ND-V (d) ND-F

Fig. 14. Different constrains of overhang edge

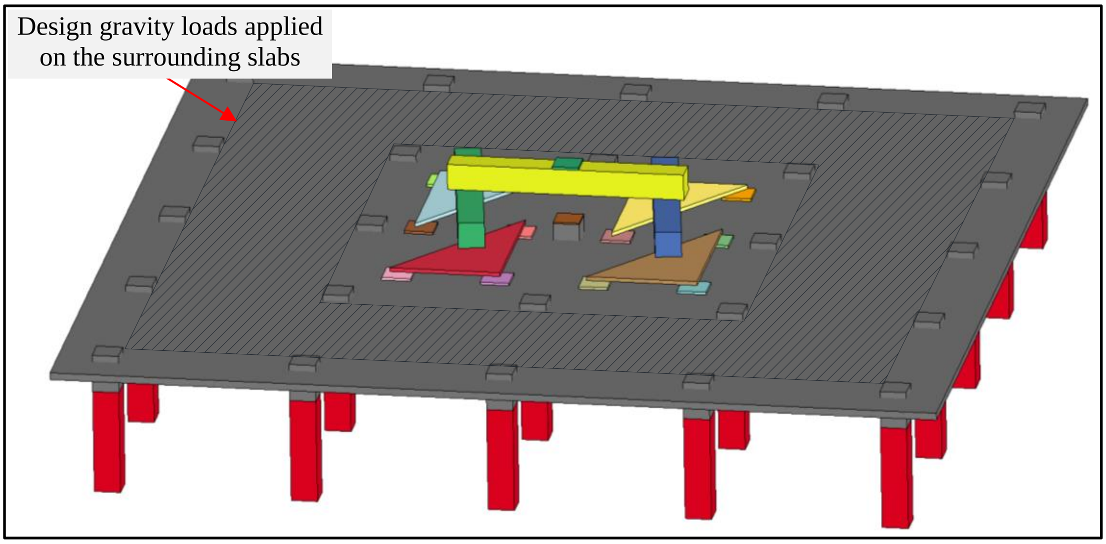

Fig. 15. Numerical model of ND-R

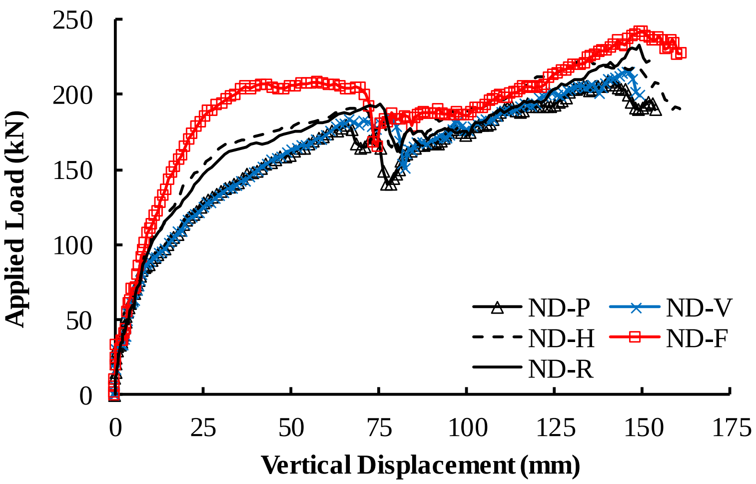

Fig. 16. Comparison of load-displacement curve of ND with varying constraints

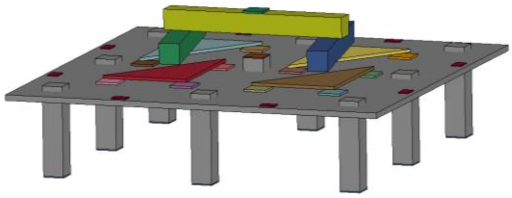

(a) ND-1F

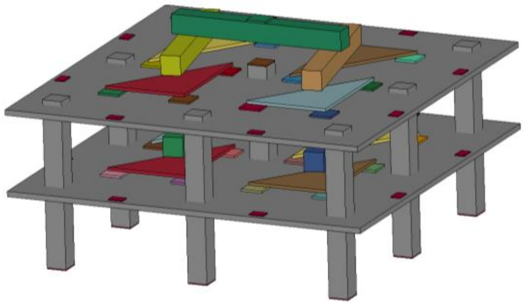

(b) ND-2F

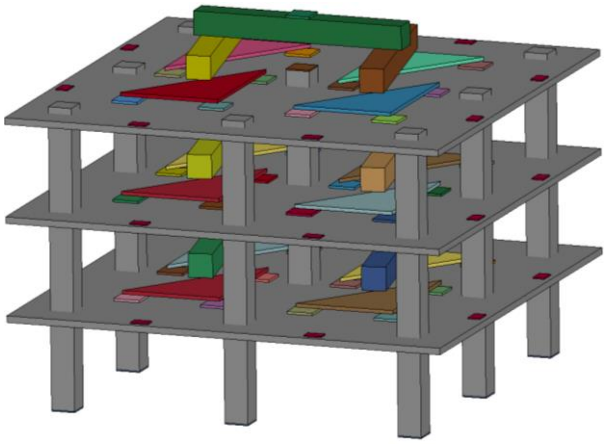

(c) ND-3F

Fig. 17. Numerical models of multi-story RC flat slab substructures

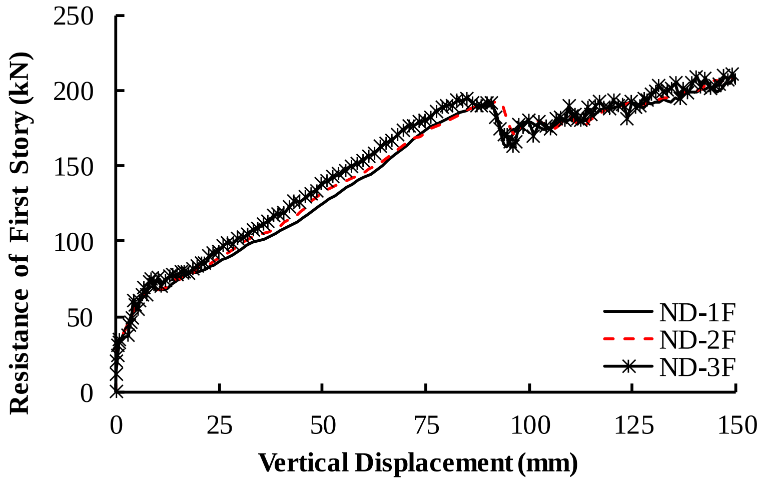

Fig. 18. Comparison of resistance in the first story of the multi-story RC flat slab substructures

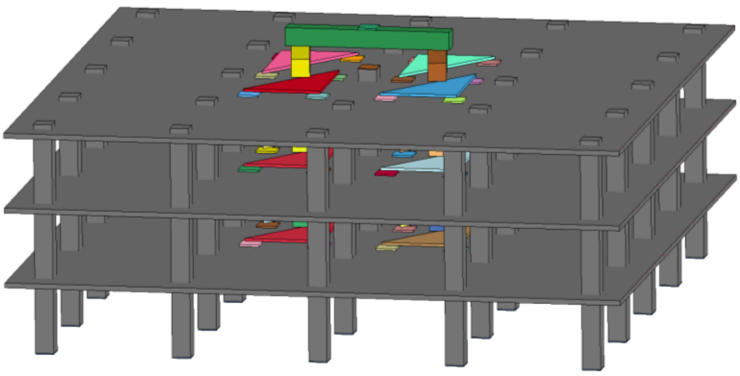

Fig. 19. Numerical models of ND-3F-R

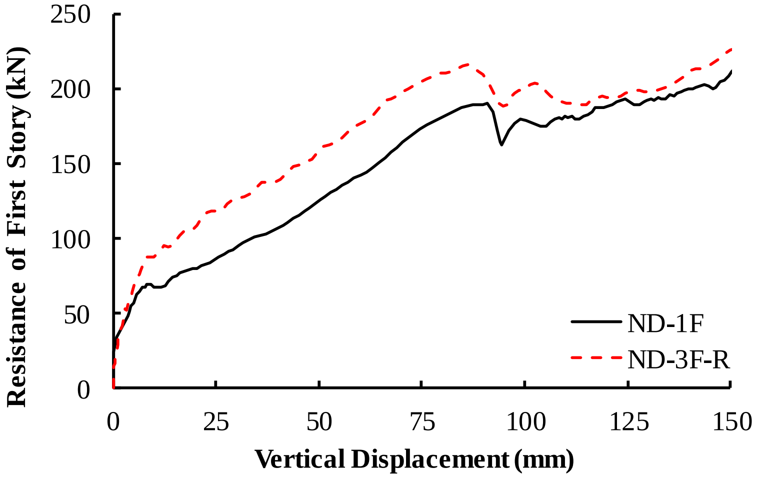

Fig. 20. Comparison of the load resistance of the first story from ND-1F and ND-3F-R

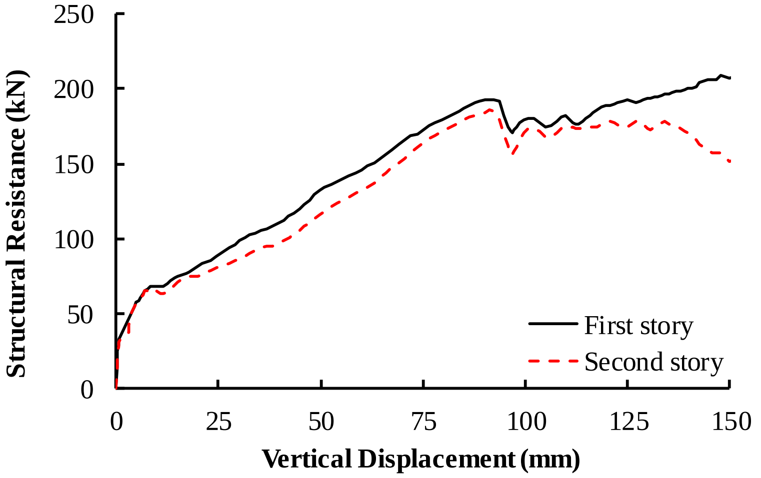

(a) ND-2F

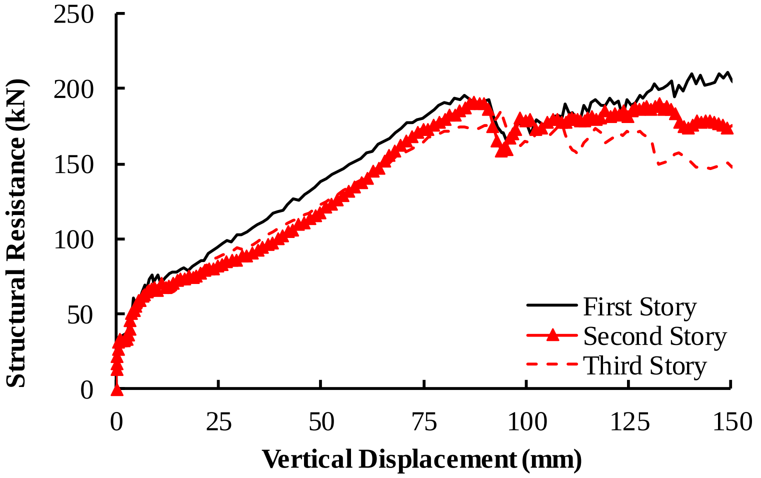

(b) ND-3F

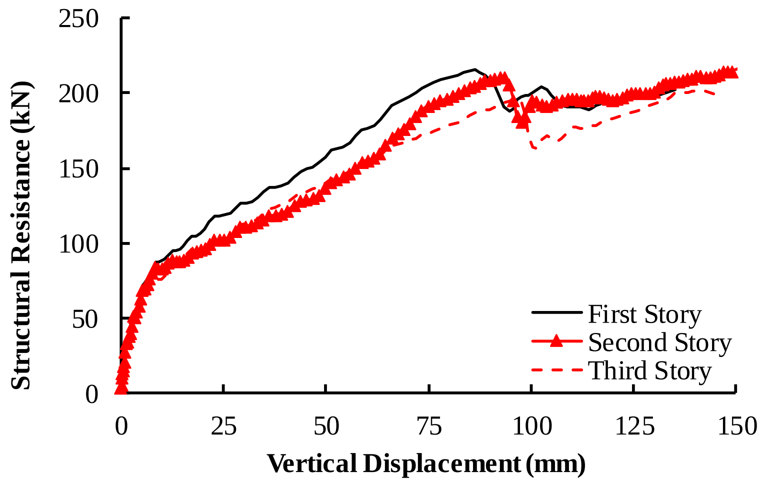

(c) ND-3F-R

Fig. 21. Comparison of the load resistance from different stories

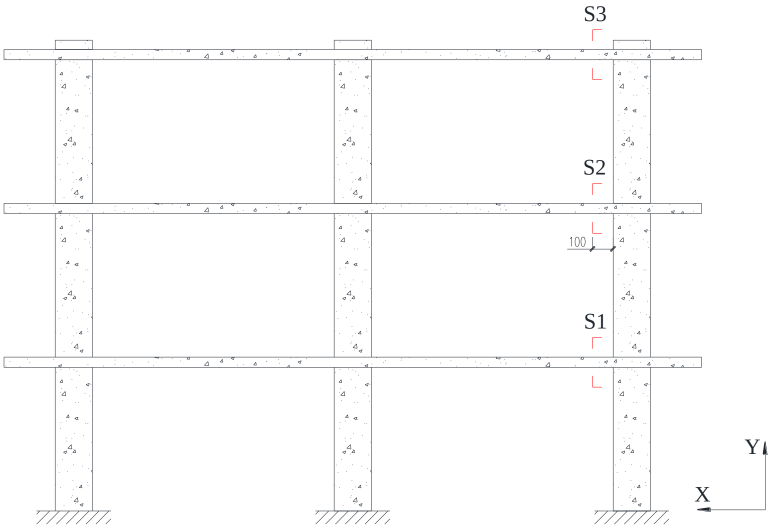

Fig. 22. Locations of slab sections

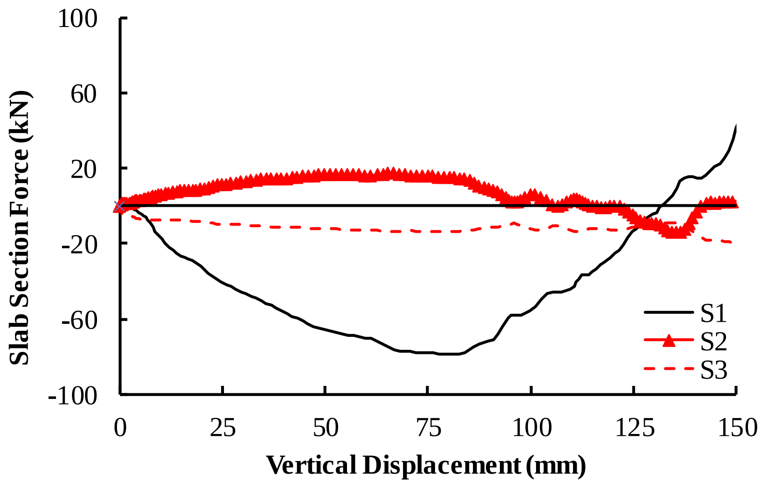

Fig. 23. Comparison of the in-plane force in x direction

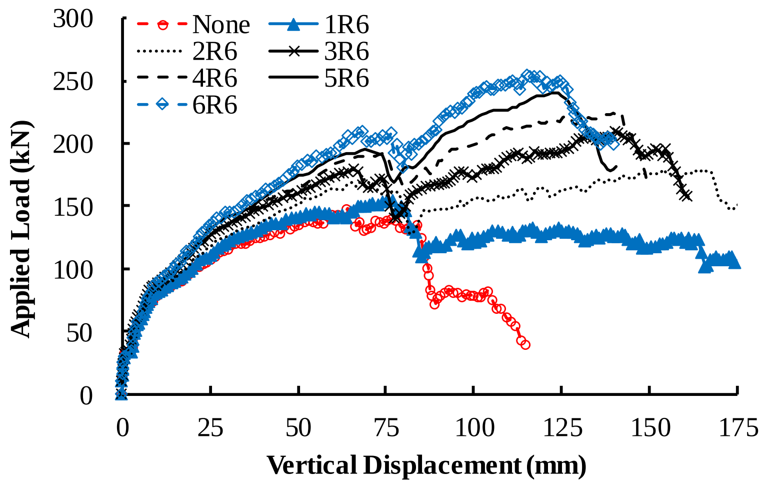

Fig. 24. Comparison of ND with different number of integrity reinforcements

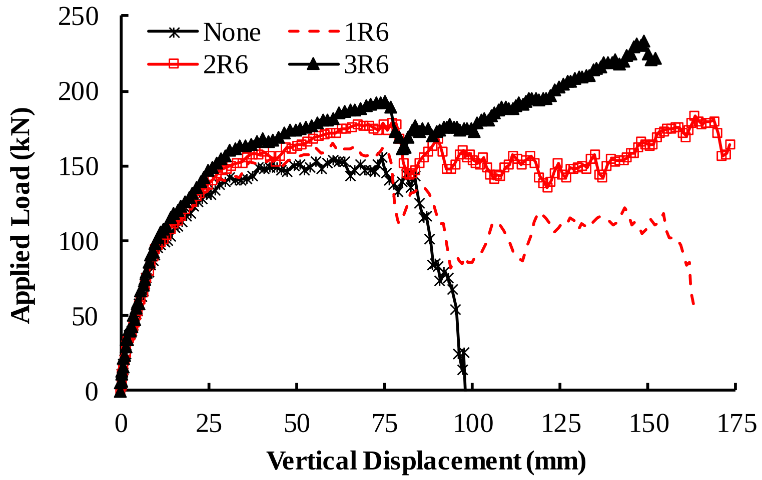

Fig. 25. Comparison of ND-R with different number of integrity reinforcements

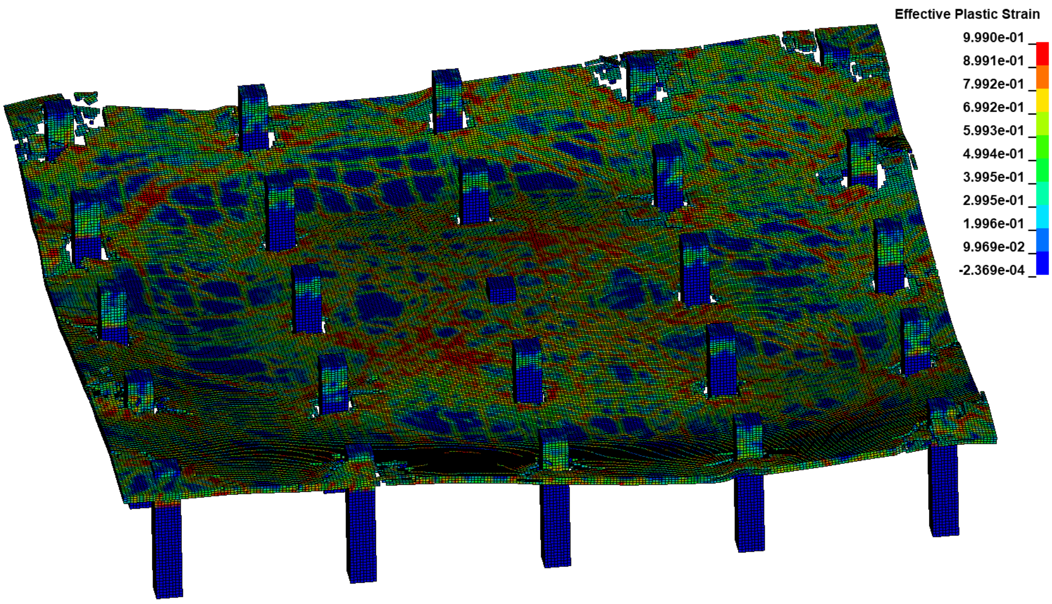

Fig. 26. Failure mode of ND-R without integrity reinforcement

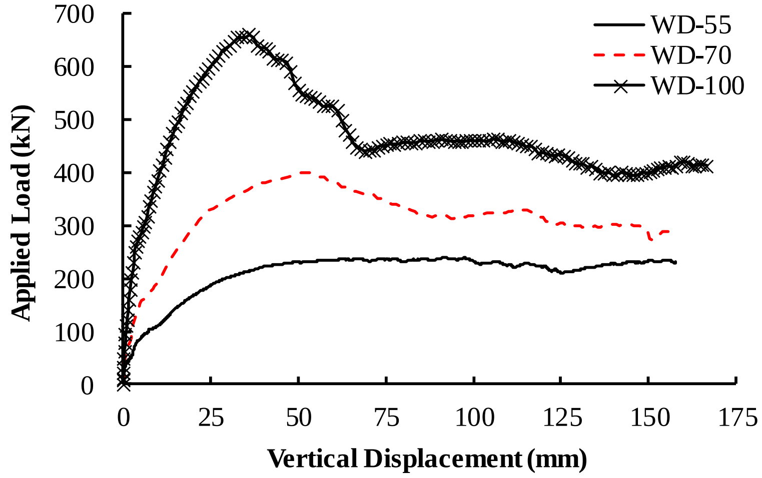

(a) WD-series

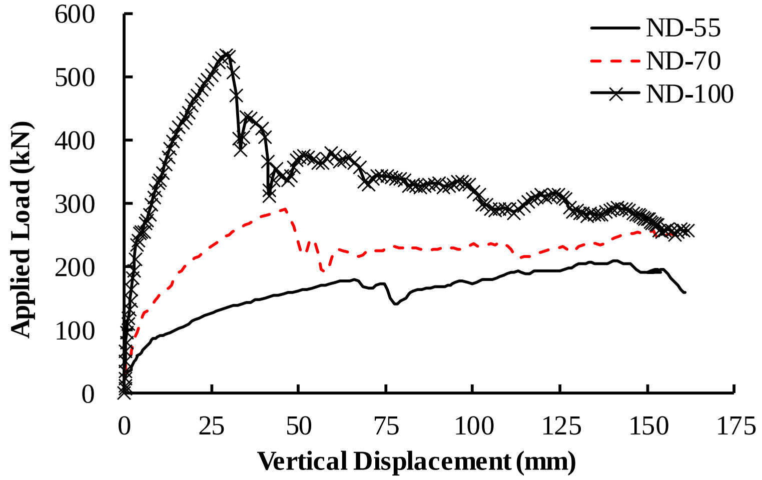

(b) ND-series

Fig. 27. Investigation on effects of slab thickness

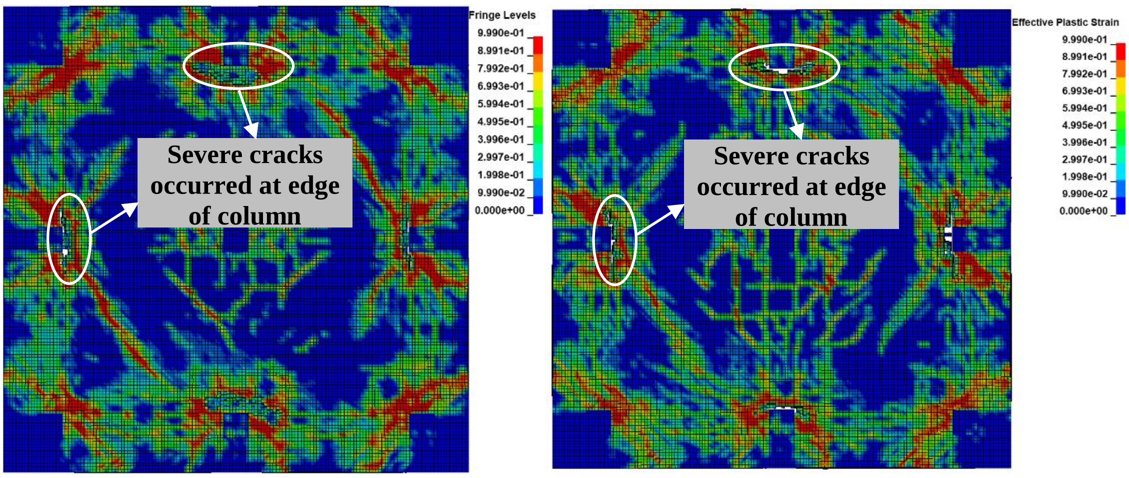

(a) WD-70 (b) WD-100

Fig. 28. Failure modes of WD-70 and WD-100